



ELSEVIER

Available online at www.sciencedirect.com

SCIENCE @ DIRECT®

Journal of Computational Physics xxx (2003) xxx–xxx

JOURNAL OF
COMPUTATIONAL
PHYSICSwww.elsevier.com/locate/jcp

A new first kind boundary integral formulation for the Dirichlet-to-Neumann map in 2D

Patrick Guidotti *

Department of Mathematics, University of California, 103 Science and Technology Bldg., Irvine, CA 92697-3785, USA

Received 5 September 2002; received in revised form 12 March 2003; accepted 13 May 2003

7 Abstract

8 In this paper, we analyze the Dirichlet-to-Neumann (DtN) operator in the periodic case as a pseudodifferential
9 operator represented through boundary integrals. We begin with some analytical results concerning the structure of the
10 operator. In particular we exploit the freedom available in the choice of the kernel for the boundary integral repre-
11 sentation to introduce a new logarithmic kernel for the fundamental solution of the Laplacian on a cylinder. We then
12 use it to develop a superalgebraically convergent numerical method to compute DtN which proves very stable even for
13 nonsmooth and large variation curves. An important step in the proposed procedure is the inversion of an integral
14 equation of first kind. To deal with it, we introduce an efficient FFT-based preconditioner which performs well in
15 combination with Nystrom's method and a decomposition of the operator based on "flat geometry subtraction".
16 © 2003 Elsevier B.V. All rights reserved.

17 *Keywords:* Dirichlet-to-Neumann Operator; Superalgebraic convergence; Boundary integral method; Fourier analysis; Integral
18 equation of first kind; Preconditioning

19 1. Introduction

20 A large variety of classical problems of mathematical physics lead to systems often comprising simple
21 potential equations in domains with nontrivial geometries and nonhomogeneous boundary data. A typical
22 situation is given when one is interested in computing a boundary force in terms of the normal derivative of
23 a potential for which Dirichlet data are known. This happens for fixed and moving boundary value
24 problems in electro-magnetism, fluid dynamics and solid mechanics (cf. for instance [1,2,5,11,13]). It also
25 naturally arises when one introduces artificial boundaries for the numerical purpose of solving problems in
26 unbounded domains (cf. [7] for instance).

27 Solving the Dirichlet problem in a bounded or unbounded domain in order to compute the normal
28 derivative of the solution on the boundary precisely defines what is known as the Dirichlet-to-Neumann

*Tel.: +1-949-824-1266; fax: +1-949-824-7993.

E-mail address: gpatrick@math.uci.edu.

29 map (DtN operator) in the literature, see [14]. The DtN operator is particularly easy to deal with if the
30 domain has a simple geometry but its efficient computation rapidly becomes challenging if the domain
31 geometry significantly deviates from a simple one. Complicated or nonsmooth geometries are very natural
32 especially in electro-magnetic scattering problems or in free boundary problems of fluid and solid me-
33 chanics. Whence the need of finding efficient and simple ways to compute the DtN operator which are as
34 much as possible insensitive to domain geometry. To keep the presentation short we restrict our attention
35 to Laplace's equation only.

36 1.1. What is known?

37 There are essentially two approaches that have been taken to computing the DtN operator: perturbative
38 pseudo-differential operator techniques and so-called boundary integral methods.

39 The first is perturbative in nature. It relies on an old result by Coifman and Meyer [3] which shows
40 analytic dependence of the DtN operator on the curve/surface in a Lipschitz neighborhood of a flat curve/
41 surface. This approach is used for instance in [5]. The nonconstant coefficient Fourier symbol for the
42 perturbed DtN operator is developed in a power series for the function representing the curve, which in
43 particular needs to be of graph type. By truncating the series, the actual problem is then reduced to
44 computing a finite linear combination of compositions of multiplication operators and constant coefficient
45 pseudodifferential operators the symbol of which can be obtained analytically. Either type of operator can
46 then be computed efficiently in physical and in Fourier space, respectively. A recent paper by Nicholls and
47 Reitich [14] gives a nice overview of these methods and improves on some of their features. In particular
48 these perturbative methods tend to be numerically unstable even for smooth curves due to analytical
49 cancellation effects in the terms of the series expansion. Nicholls and Reitich [14] show how these methods
50 can be made more stable by eliminating cancellation effects taking into account a higher computational cost
51 and some analytical manipulations.

52 The second is based on classical boundary integral representations for the solution using single and
53 double layer potentials. This technique can be used for a variety of different problems. The knowledge of a
54 fundamental solution for the potential equation in free space allows one to derive a relation (using Green's
55 formula, see for instance [9]) between Dirichlet and Neumann boundary data for a harmonic function of
56 the interior. This approach, implemented for instance in [1,2] has the advantage of applying to general
57 curves. In particular they need not be of graph type. At the same time it prevents the use of Fourier ar-
58 guments precisely because it can handle very general geometries which are not even close to being linear/
59 circular. Another price which needs to be paid is that the integral equations have singular or weakly sin-
60 gular kernels, which is a real numerical issue especially for surfaces in \mathbb{R}^3 . These methods would also profit
61 from an improvement of their numerical stability. In [8] the authors give a nice general overview of the use
62 of boundary integral methods in applied mathematics, especially in fluid dynamics.

63 1.2. What is new?

64 Our program is to first consider the problem of finding a satisfactory analytical representation for the
65 DtN operator and subsequently to use it in order to obtain a good discretization. In order to do so we
66 derive a new kernel of logarithmic type for the fundamental solution for the Laplace operator on an cyl-
67 nder. With it we propose a single-layer potential boundary integral method for the computation of DtN.
68 The procedure entails solving an integral equation of first kind. The discretized equations will inherit the ill-
69 posedness of their continuous counterpart and suffer from the presence of singular integrals. We show how
70 the difficulties stemming from these can be elegantly circumvented by using a boundary integral method
71 combined with Fourier analysis, however not in a perturbative way. More specifically we propose a FFT-
72 based preconditioner, which, combined with the standard flat geometry subtraction, eventually leads to a

73 superalgebraically convergent scheme for the computation of DtN. Our final product will be an accurate
 74 and stable pseudo-spectral (Fourier) boundary integral method which performs equally well for nonsmooth
 75 and/or large variation curves as it does for small variation smooth curves. The ideas can readily be applied
 76 to the analogous 3D problem but will be the topic of another paper.

77 The rest of the paper is organized as follows. In Section 2, we perform all the preparatory analytical work.
 78 We in particular set up a bridge between the boundary integral method and the Fourier method. In Section 3,
 79 we introduce a discretization of the analytical representations by means of Nystrom’s method combined with
 80 the choice of optimal quadrature rules and with a FFT-based preconditioner. Finally Section 4 is devoted to
 81 numerical experiments in support of our theoretical claims. In Appendix A, we give a proof of the jump
 82 relation satisfied by the integral representations based on the new kernel. In Appendix B, we show how the
 83 nonconstant coefficient symbol of the general representation can be derived from the “flat” symbol.

84 2. Analysis of the DtN operator

85 In this paper, we concentrate our attention on the 2D periodic situation. More precisely we consider
 86 Laplace’s equation

$$-\Delta u = 0 \quad \text{in } \Omega_\Gamma, \quad u = g \quad \text{on } \Gamma \quad (2.1)$$

88 in the region Ω_Γ lying above the 1-periodic curve Γ . Although the results presented here remain valid in the
 89 case of general curves we restrict ourselves to the case of curves which can be represented as the graph of a
 90 function for the sake of simplicity. For the general case we refer to Remark 5 in Section 2.3 and the nu-
 91 merical experiments of Section 4 (cf. Examples 4 and 8). We propose the new kernel

$$G(x, y) = \frac{1}{2\pi} \ln(1 + e^{-4\pi y} - 2 \cos(2\pi x) e^{-2\pi y}), \quad (2.2)$$

93 which is 1-periodic in the first variable, and the corresponding representation for the solution u_g of (2.1) of
 94 the form

$$u_g(z) = \int_\Gamma G(z - \bar{z}) f(\bar{z}) d\sigma_\Gamma(\bar{z}), \quad z \in \Omega_\Gamma \quad (2.3)$$

96 in terms of an unknown boundary function f . If we assume that the curve Γ be parametrized by the 1-
 97 periodic function s , the integral (2.3) reads

$$u_g(x, y) = \int_0^1 G(x - \tilde{x}, y - s(\tilde{x})) f(\tilde{x}) \sqrt{1 + s_x^2(\tilde{x})} d\tilde{x}, \quad (x, y) \in \Omega_\Gamma. \quad (2.4)$$

99 Since we are eventually interested in the derivative in normal direction restricted to the boundary we
 100 assume the boundary value g has mean zero, that is,

$$\int_\Gamma g(\bar{z}) d\sigma_\Gamma(\bar{z}) = 0. \quad (2.5)$$

102 It has indeed been shown (see for instance [16]) that the kernel of DtN consists of mean zero boundary
 103 functions in a variety of functions spaces comprising $L_2(\Gamma)$ for a simple example. Assumption (2.5) also
 104 makes

$$g = \left(\int_\Gamma G(\cdot - \bar{z}) f(\bar{z}) d\sigma_\Gamma(\bar{z}) \right) \Big|_\Gamma$$

106 uniquely solvable. Let ν denote the unit outer normal to Ω . After finding the boundary function f we use
 107 (2.4) to derive a boundary integral representation of $\text{DtN}(g) = \partial_\nu u_g|_\Gamma$ (the restriction might occasionally
 108 need to be understood in the sense of traces) as follows

$$\text{DtN}(g)(z) = \left(\int_\Gamma (\nabla G(z - \tilde{z})|_\nu(z)) f(\tilde{z}) d\sigma_\Gamma(\tilde{z}) \right) \Big|_\Gamma \quad (2.6)$$

110 or, in coordinates,

$$\text{DtN}(g)(\tilde{x}) = \left(\int_0^1 K(x, \tilde{x}) f(\tilde{x}) \frac{\sqrt{1 + s_x^2(\tilde{x})}}{\sqrt{1 + s_x^2(x)}} d\tilde{x} \right) \Big|_{y=s(x)} \quad (2.7)$$

112 for

$$K(x, \tilde{x}) = \partial_x s(x) \partial_x G(x - \tilde{x}, y - s(\tilde{x})) - \partial_y G(x - \tilde{x}, y - s(\tilde{x})).$$

114 We defined the function u_g only above the curve Γ and it is therefore clear that the above restrictions are
 115 always meant to be obtained by taking the limit from above the curve Γ . In view of the singularity of kernel
 116 (2.2) a singular interaction along the boundary curve will in fact produce a Dirac contribution as we shall
 117 see below.

118 2.1. Derivation of the kernel

119 Let us start with the trivial case, where the curve Γ is the x -axis. It is natural to look for a solution in
 120 Fourier space and, since we are focussing on the periodic case, we obviously easily obtain the standard
 121 representation for the solution of (2.1)

$$u_g(x, y) = \sum_{k=-\infty}^{\infty} \hat{g}_k e^{-2\pi|k|y} e^{2\pi i k x} \quad (2.8)$$

123 in terms of the Fourier coefficients of the boundary function g . From (2.8) we can trivially compute

$$\text{DtN}(g) = 2\pi \sum_{k=-\infty}^{\infty} |k| \hat{g}_k e^{-2\pi|k|y} e^{2\pi i k x} \Big|_{y=0}.$$

125 But this is not the way we want to look at the above formulas. We actually want to take a more abstract
 126 perspective based on pseudo differential operators (Ψ DOs in the sequel) techniques. If we view

$$(e^{-2\pi|k|y})_{k \in \mathbb{Z}}$$

128 as the symbol of a Ψ DO with constant coefficients (depending on the parameter $y > 0$) we can actually
 129 compute the kernel of the corresponding convolution operator associated to (2.8) (at least for fixed y) to
 130 obtain

$$H(x, y) = \sum_{k=-\infty}^{\infty} e^{-2\pi|k|y} e^{2\pi i k x} = \frac{2 - 2e^{-2\pi y} \cos(2\pi x)}{1 + e^{-4\pi y} - 2 \cos(2\pi x) e^{-2\pi y}} - 2, \quad (2.9)$$

132 where H is nothing but a harmonic function of the upper/lower half plane for which

$$\lim_{y \rightarrow 0^+} H(\cdot, y) = \delta - 1 \text{ in } \mathcal{D}'_p(0, 1),$$

134 where we introduce the space

$$\mathcal{D}'_p(0, 1) = \mathcal{L}\left(C_p^\infty(0, 1), \mathbb{K}\right)$$

136 of 1-periodic distributions over the line as the dual of 1-periodic test functions with its natural (locally
137 convex) Fréchet topology. Let us introduce a 1-periodic convolution through

$$(u * _p v)(x) = \int_0^1 u(x - \tilde{x})v(\tilde{x}) d\tilde{x}, \quad x \in (0, 1), \quad (2.10)$$

139 which is easily checked to be well-defined by thinking of u as being periodically extended outside $(0, 1)$ in
140 order to make sense of $u(x - \tilde{x})$. Alternatively, if we prefer the comfort of working solely in one periodicity
141 interval, we can interpret the sum $x - \tilde{x}$ as a sum modulo the period. In this new notation, the unique
142 bounded solution to the periodic Poisson equation is seen to be given by

$$u_g(x, y) = (H(\cdot, y) * _p f)(x) = \int_0^1 H(x - \tilde{x}, y)f(\tilde{x}) d\tilde{x}, \quad (2.11)$$

144 which is nothing else but the periodic version of the well-known Poisson integral. We can therefore rein-
145 terpret the computation of DtN(g) in this case as first solving the convolution equation

$$\int_0^1 H(x - \tilde{x}, 0)f(\tilde{x}) d\tilde{x} = \langle \delta_{(x-\cdot)} - 1, f \rangle = g(x), \quad x \in (0, 1), \quad (2.12)$$

147 which is trivially solved by $f = g$ (recall that g is assumed to have mean zero) and then computing

$$\partial_y u_g(x) = -\lim_{y \rightarrow 0} \int_0^1 \partial_y H(x - \tilde{x}, y)f(\tilde{x}) d\tilde{x} = -(H_y(\cdot, 0) * _p f)(x) = f(x), \quad (2.13)$$

149 which is a boundary representation of the derivative in normal direction of u_g . Although this is a perfectly
150 valid analytic representation, the kernel $\partial_y H(\cdot, 0)$ is unfortunately hypersingular and won't provide a viable
151 computational recipe. With this new point of view, though, we are now able to avoid dealing with hy-
152 persingular kernels directly. Eq. (2.12) is a mere instance of a variety of other possible superpositions of
153 harmonic functions. We can, for instance, use the alternative kernel G obtained by integrating (2.9) with
154 respect to the y -variable. It coincides with (2.2) and is clearly again a x -periodic harmonic function. A
155 contour plot of G is shown in Fig. 1 together with its continuous counterpart. Using (2.2) we represent the
156 solution of Laplace's equation through

$$u_g(x, y) = \int_0^1 G(x - \tilde{x}, y)f(\tilde{x}) d\tilde{x} \quad (2.14)$$

158 and finding f by imposing the boundary condition

$$\int_0^1 G(x - \tilde{x}, 0)f(\tilde{x}) d\tilde{x} = g(x), \quad x \in (0, 1), \quad (2.15)$$

160 which is an integral equation of the first kind with a less singular kernel than (2.12) and, eventually
161 computing

$$-\lim_{y \rightarrow 0} \int_0^1 \partial_y G(x - \tilde{x}, y)f(\tilde{x}) d\tilde{x} = -\int_0^1 H(x - \tilde{x}, 0)f(\tilde{x}) d\tilde{x} = -f(x). \quad (2.16)$$

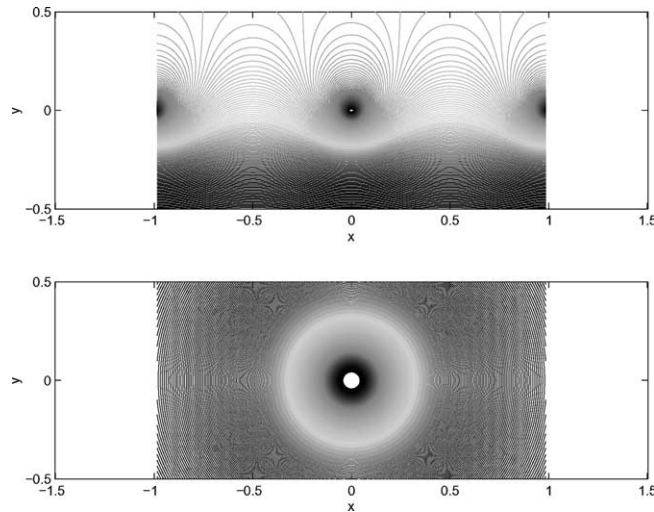


Fig. 1. A contour plot of G and $\frac{1}{\pi} \log(x^2 + y^2)$.

Remark 1. Using representation (2.14) instead of (2.11) corresponds to using the fundamental solution $\frac{1}{2\pi} \ln |(x, y)|$ instead of the Poisson integral to represent the solution in the continuous nonperiodic case.

Remark 2. Kernel (2.2) also has the advantage of avoiding the standard reduction to the continuous case via Poisson’s summation formula by dealing with the symbol directly. This point of view will be beneficial when choosing the discretization in Section 3.

Remark 3. We point out that the choice of the kernel G is not unique. In fact, we could have obtained smoother kernels by modifying the symbol of G to, for instance,

$$\sum_{n=-\infty}^{\infty} \frac{e^{-2\pi|k|y}}{(2\pi|k|)^p} e^{2\pi i k x}$$

for some power $p > 1$ or more general symbols still. Here we only remark that an important feature of any possible alternative kernel is that it should contain all modes of decay as in the example chosen above. Appropriate “reflection properties” need also to be derived for the kernel in order to be able to define the symbol in the lower half plane. See Appendix B for more details about this.

Taking this perspective we can now introduce an associated boundary integral method and still recognize its relation to the Fourier method. This will be of utmost importance in the choice of the numerical scheme to actually perform the computations (see Sections 3 and 4).

2.2. A boundary integral method

Assume that the boundary curve Γ is parametrized by the periodic continuously differentiable function

$$s \in C^1([0, 1), \mathbb{R}). \quad (2.17)$$

This assumption can be weakened but, since we are not interested in the optimal analytical result here, we shall not elaborate on that. Then we use kernel (2.2) and superpose translated copies of it along the curve Γ to obtain a x -periodic harmonic function u given by

$$u(x, y) = \int_0^1 G(x - \tilde{x}, y - s(\tilde{x})) f(\tilde{x}) \sqrt{1 + s_x^2(\tilde{x})} d\tilde{x} \quad (2.18)$$

185 for a suitable function $f \in L_{2,p}$. The latter is the Banach space of 1-periodic square integrable functions. If
186 we choose the boundary function $g \in H_p^1$ with vanishing mean, then

$$\int_0^1 G(x - \tilde{x}, s(x) - s(\tilde{x})) f(\tilde{x}) \sqrt{1 + s_x^2(\tilde{x})} d\tilde{x} = g(x) \quad (2.19)$$

188 has a unique mean zero solution $f \in L_{2,p}$. We can then use (2.18) to obtain a boundary integral
189 representation for DtN(g). Since

$$\nabla G(x, y) = \left(\frac{4 \cos(\pi x) \sin(\pi x)}{2 \cosh(2\pi y) - 2 \cos(2\pi x)}, \frac{2 - 2e^{-2\pi y} \cos(2\pi x)}{1 + e^{-4\pi y} - 2 \cos(2\pi x)e^{-2\pi y}} - 2 \right) \quad (2.20)$$

191 and therefore

$$\nabla G(x, 0) = \left(v.p. \frac{\cos(\pi x)}{\sin(\pi x)}, \delta - 1 \right), \quad (2.21)$$

193 some care is needed in deriving the boundary integral representation. The result is contained in the fol-
194 lowing lemma.

195 **Lemma 4.** *Assume that $s \in C_p^1([0, 1])$, then the following holds*

$$\int_{\Gamma} \partial_{v(z)} G(z - \tilde{z}) f(\tilde{z}) d\sigma_{\Gamma}(\tilde{z}) \quad (2.22)$$

↓

$$-f(z_0) + v.p. \int_{\Gamma} \partial_{v(z_0)} G(z_0 - \tilde{z}) f(\tilde{z}) d\sigma_{\Gamma}(\tilde{z})$$

199 as

$$(x, y) = z \rightarrow z_0 = (x_0, s(x_0)), \quad (x, y) \in \Omega_{\Gamma}$$

201 if the limit is not taken tangentially to the boundary curve.

202 **Proof.** See Appendix A. \square

203 We use the above formula in the discretizations of Section 3.

204 2.3. Decomposition of the integral equation

205 In this section, we present an analytic decomposition/factorization of Eq. (2.19) which will eventually be
206 mimicked in the discretization. We introduce the symbols

$$a_0 = (2\pi|k|)_{k \in \mathbb{Z}^*}, \quad g_0 = (1/2\pi|k|)_{k \in \mathbb{Z}^*}$$

208 corresponding to the operators on the flat periodic geometry, where we used the standard notation
209 $\mathbb{Z}^* := \mathbb{Z} \setminus \{0\}$. We further need the nonconstant coefficient symbol

$$\left(g_s(k, x, \tilde{x})\right)_{k \in \mathbb{Z}^*} \quad (2.23)$$

211 corresponding to the kernel appearing in (2.19). We refer to Appendix B for a formula (see (B.2) and (B.3))
 212 and for its derivation. Denoting the Fourier transform by

$$(\mathcal{F}_{x \rightarrow k} u)(k) = \int_0^1 e^{-2\pi i k x} u(x) dx, k \in \mathbb{Z},$$

214 it is natural to decompose

$$\mathcal{F}_{k \rightarrow \tilde{x}}^{-1} g_s(\cdot, x, \tilde{x}) \mathcal{F}_{x \rightarrow k}$$

216 as follows

$$\mathcal{F}_{k \rightarrow \tilde{x}}^{-1} g_0 \mathcal{F}_{x \rightarrow k} + \mathcal{F}_{k \rightarrow \tilde{x}}^{-1} [g_s(\cdot, x, \tilde{x}) - g_0] \mathcal{F}_{x \rightarrow k}. \quad (2.24)$$

218 Following the procedure outlined in the previous subsection we utilize this decomposition in dealing with
 219 (2.19).

220 We shall see that most (numerical) ill-conditioning can essentially be confined to the constant coefficient
 221 term in this formulation and show how to get rid of it in a way which transforms (2.19) into an equation of
 222 second kind. From the analytical point of view we proceed as follows. Denote the integral operator with
 223 symbol b by $\text{op}(b)$. Then (2.24) simply reads

$$\text{op}(g_s) = \text{op}(g_0) + \text{op}(g_s - g_0)$$

225 it is easy to see that

$$\text{op}(a_0) \text{op}(g_s) = \text{id} - I_\Gamma + \text{op}(a_0) \text{op}(g_s - g_0) \quad (2.25)$$

227 for

$$I_\Gamma(u) = \int_\Gamma u(\tilde{z}) d\sigma_\Gamma(\tilde{z}).$$

229 Therefore, if we restrict our attention to mean zero functions, as we do, (2.25) simply reads

$$\text{op}(a_0) \text{op}(g_s) = \text{id} + \text{op}(a_0) \text{op}(g_s - g_0). \quad (2.26)$$

231 It turns out that this point of view is very beneficial when choosing the appropriate discretization to be
 232 used. In particular we base our discretization on the following “mixed” reformulation of (2.19) obtained
 233 using (2.26)

$$\text{op}(a_0)g = f + \text{op}(a_0) \int_0^1 k(x, \tilde{x}) f(\tilde{x}) d\tilde{x} \quad (2.27)$$

235 for

$$K(x, \tilde{x}) = G\left(x - \tilde{x}, s(x) - s(\tilde{x})\right) \sqrt{1 + s_x^2(\tilde{x})} - G(x - \tilde{x}, 0). \quad (2.28)$$

237 The above factorization of the operator essentially shows that, in order to solve (2.19), one can solve

$$\text{op}(g_0)g = f$$

239 instead, that is, consider g and f as if they were defined on a flat domain, and subsequently apply a
 240 “bounded” correction to the result. Eq. (2.27) looks very much like an integral equation of the second

241 kind. Its kernel is not explicitly known, however, since it is given by the DtN value of $K(\cdot, \tilde{x})$ for
242 $\tilde{x} \in (0, 1)$.

243 **Remark 5.** It is an important observation that we do not need the boundary curve to be of graph type. In
244 fact, if

$$(x, y) : (0, 1) \rightarrow \mathbb{R}^2, \quad \alpha \mapsto (x(\alpha), y(\alpha))$$

246 is the parametrization (with parameter interval normalized to $(0, 1)$) of an admissible “periodic” curve Γ ,
247 that is, a, at least Lipschitz, curve with

$$x(0) = 0, \quad x(1) = 1, \quad y(1) = y(0),$$

249 we can use the corresponding boundary representations

$$\int_0^1 G(x(\beta) - x(\alpha), y(\beta) - y(\alpha)) f(x(\alpha), y(\alpha)) \sqrt{x_\alpha^2(\alpha) + y_\alpha^2(\alpha)} \, d\alpha = g(x(\beta), y(\beta)) \quad (2.29)$$

251 to determine the intermediate function f and, since Lemma 4 remains valid for such curves, obtain

$$(\text{DtN}_{\Gamma} g)(x(\beta), y(\beta)) = -f(x(\beta), y(\beta)) + v.p. \int_0^1 K(\beta, \alpha) f(x(\alpha), y(\alpha)) \sqrt{\frac{x_\alpha^2(\alpha) + y_\alpha^2(\alpha)}{x_\alpha^2(\beta) + y_\alpha^2(\beta)}} \, d\alpha \quad (2.30)$$

253 with

$$K(\beta, \alpha) = -x_\beta(\beta) \partial_y G(x(\beta) - x(\alpha), y(\beta) - y(\alpha)) + y_\beta(\beta) \partial_x G(x(\beta) - x(\alpha), y(\beta) - y(\alpha)).$$

255 The same decomposition of the operator described above is possible and leads to numerical benefits in this
256 case, too. We shall come back to this in the section dedicated to numerical experiments (see Examples 4 and
257 8).

258 3. The discretization

259 We now turn to the actual numerical computation of DtN. In doing so we follow the procedure outlined
260 in the previous sections. We discretize the periodicity interval $[0, 1)$ at equidistant points

$$x_j = (j - 1)h, \quad j = 1, \dots, 2^m + 1 =: n \quad \text{for } h = 2^{-m} \text{ and } m \in \mathbb{N}.$$

262 Having fixed the discretization we denote the Fast Fourier Transform of a vector $f \in \mathbb{C}^n$ by $\mathcal{F}_m f$. If we
263 write \mathcal{F}_m only, we mean the representation matrix of the FFT in the natural basis of \mathbb{C}^n . First we need to
264 take a look at (2.27) in order to determine the intermediate vector f . We take

$$\text{op}_m(a_0) = \mathcal{F}_m^{-1}(P_m a_0) \mathcal{F}_m \quad (3.1)$$

266 as a discretization of $\text{op}(a_0)$ where of course

$$(P_m a_0) = \text{diag} \left[(2\pi|k|)_{|k| \leq 2^{m-1}} \right].$$

268 Next we discretize the remaining integral operator in (2.27) by using the trapezoidal rule to obtain

$$A_m(j, k) = h(G(x_j - x_k, s_j - s_k) - G(x_j - x_k, 0)), \quad j, k = 1, \dots, 2^m, \quad (3.2)$$

270 where $(s_j)_{j=1,\dots,2^m}$ is the discretization of the function s we use to describe the boundary of Γ . Taking into
 271 account the asymptotic behavior of G into the singularity (cf. (2.21)) and the logarithmic nature of G we
 272 compute the difference $A_m(j, k)$ as

$$A_m(j, k) = \frac{1}{2\pi} \log \left[1 + \frac{a_m(j, k)}{b_m(j, k)} \right], \quad j \neq k$$

274 for

$$\begin{aligned} a_m(j, k) &= e^{-4\pi(s_j - s_k)} - 1 = -2(e^{-2\pi(s_j - s_k)} - 1) \cos(2\pi(x_j - x_k)) \\ b_m(j, k) &= 2 - 2 \cos(2\pi(x_j - x_k)) \end{aligned}$$

276 and

$$A_m(j, j) = \frac{1}{2\pi} \log \left[1 + (s_x)_j^2 \right]$$

278 on the diagonal. We end up with a discretized equation for the vector

$$\tilde{f}_j^m = f_j^m \sqrt{1 + (s_x)_j^2}, \quad j = 1, \dots, 2^m$$

280 in the form

$$(\text{id}_m + \text{op}_m(a_0)A_m)\tilde{f}^m = \text{op}_m(a_0)g^m. \quad (3.3)$$

Remark 6. At first sight it might appear that a good reason for subtracting the flat term in (3.2) be that it
 283 helps taking care of the singularity on the diagonal. Although this is certainly true, another benefit is ac-
 284 tually the significant reduction of the condition number. We refer the reader to the next section for nu-
 285 merical examples illustrating this fact. From the analytical point of view, we observe that

$$\text{op}_m(a_0)A_m$$

287 can be viewed as the discretization of a bounded operator and we therefore do not expect a deterioration of
 288 its conditioning as the mesh becomes finer.

289 At this point we compute \tilde{f}^m as

$$\tilde{f}^m = (\text{id}_m + \text{op}_m(a_0)A_m)^{-1} \text{op}_m(a_0)g^m$$

291 and proceed with the computation of $\text{DtN}(g)$. We need to evaluate integral (2.22) which we discretize by
 292 means of the spectral “alternating point” trapezoidal rule (see [15]). In order words let the kernel in (2.22)
 293 be discretized as

$$B_m(j, k) = h((s_x)_j, -1) \cdot \nabla G(x_j - x_k, s_j - s_k)$$

295 if

$$j - k = 1 \pmod{2}$$

297 and

$$B_m(j, k) = 0$$

299 otherwise. Then we compute

$$\text{DtN}_m(g_m) = -f^m + \frac{B_m \tilde{f}^m}{\sqrt{1 + (s_x)_m^2}}. \quad (3.4)$$

301 4. Numerical examples

302 In this final section, we compute a few examples to illustrate the virtues of the method developed in the
 303 previous sections. In particular we also consider curves of large variation as well as nonsmooth curves. We
 304 consider two types of examples. In a first group of examples we choose different boundary functions s and
 305 obtain test boundary functions g by using combinations of the simple x -periodic harmonic functions

$$h_k(x, y) = e^{-2\pi ky} \cos(2\pi kx). \quad (4.1)$$

307 These will provide a good test for the accuracy of our method. In the second type of examples we choose
 308 both the boundary function s and the boundary value g freely. We would not bother choosing mean zero
 309 boundary values g but take the numerical projection

$$P^m g^m = g^m - \frac{\sum_j g_j^m \sqrt{1 + (s_x)_j^2}}{\sum_j \sqrt{1 + (s_x)_j^2}}$$

311 instead, where we again discretized the integrals by the trapezoidal rule.

312 4.1. $\text{op}_m(a_0)$ is a good preconditioner

313 Although the decomposition (2.27) of the DtN operator seems natural from the theoretical point of
 314 view, it might well be numerically ineffective. We shall show that it in fact is tremendously beneficial. It
 315 turns out that $\text{op}_m(a_0)$ carries most of the ill-conditioning of the problem but poses no problem as a ΨDO
 316 with constant coefficients. To illustrate this fact we consider a series of examples. We obviously do not need
 317 to consider any boundary value to compute the condition c_0 number of

$$\text{id}_m + \text{op}_m(a_0)A_m, \quad (4.2)$$

319 which is the only matrix we actually need to invert in our procedure. If one needs to consider very fine grids
 320 the structure of (4.2) can be exploited in combination with an iterative method for the inversion: The
 321 pseudodifferential operator $\text{op}_m(a_0)$ can be dealt with in Fourier space whereas the integral operator could
 322 be tamed by multipole expansions (cf. [12]).

323 In the following examples we choose

$$m = 6, 7, 8, 9, 10.$$

325 We compare the condition number c_0 of (4.2) with the condition number c_1 of the discretization matrix
 326 $\text{bad}A$ corresponding to the nonmodified boundary integral equation (2.19) modulo the fact that we factor
 327 out the smallest eigenvalue which corresponds to the 1D kernel of the continuous operator. The boundary
 328 curves considered in Examples 1–4 (and then again in Example 5–8 again) are depicted in Figs. 2 and 3.

329 **Example 1.** Consider the smooth boundary curve given by

$$s = 0.8 + \tanh(2 + \sin(2\pi x)).$$

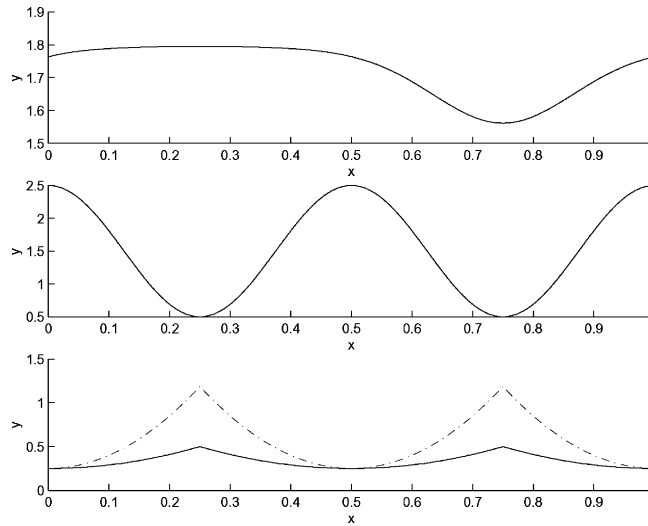


Fig. 2. The boundary curves Γ for Examples 1–3 and 5–7.

331 Table 1 contains the results obtained in this case.

332 **Example 2.** As a second example we take a curve s with a large variation given by

$$s = 0.5 + 2 \cos^2(2\pi x).$$

334 Observe that the derivative of s roughly varies between -10 and 10 . The results are summarized in Table 2.

335 **Example 3.** Finally we consider the nonsmooth Lipschitz curve

$$s = 0.25 + \alpha r$$

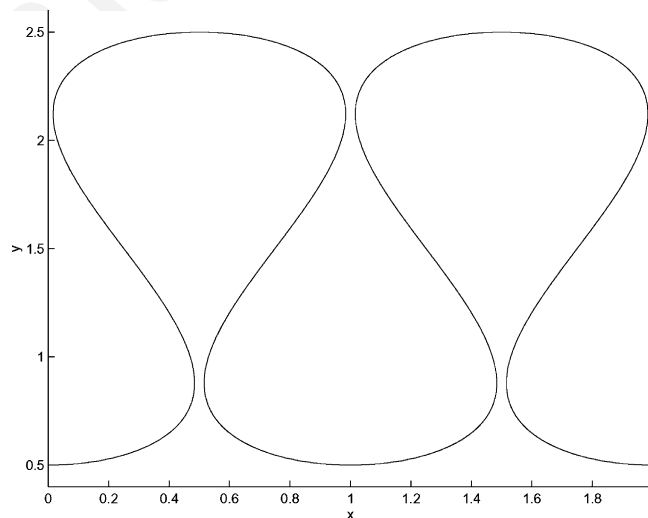


Fig. 3. Two periods of the boundary curve Γ for Example 4.

Table 1
The condition numbers for (4.2) and $badA$

	c_0	c_1
$m = 6$	1.5210	7.1795×10^2
$m = 7$	1.5210	2.0023×10^5
$m = 8$	1.5210	5.7463×10^5
$m = 9$	1.5210	1.2906×10^6
$m = 10$	1.5210	2.6674×10^6

Table 2
The condition numbers for (4.2)1 and $badA$

	c_0	c_1
$m = 6$	56.4739	3.6536×10^2
$m = 7$	56.4140	1.4635×10^3
$m = 8$	56.4139	2.5714×10^3
$m = 9$	56.4139	1.0205×10^4
$m = 10$	27.3285	3.4427×10^6

337 with

$$r = x^2 \chi_{[0,0.25)} + (0.5 - x)^2 \chi_{[0.25,0.75)} + (1 - x)^2 \chi_{[0.75,1)},$$

339 where χ_J denotes the characteristic function of the interval J and $\alpha = 4, 15$. In this case the results for $\alpha = 4$
340 are found in Tables 3 and Table 4 for $\alpha = 15$.

341 **Example 4.** Finally, we consider the case of a curve Γ which can not be represented as the graph of a
342 function (see Fig. 3). Let it be parametrized by

$$\gamma^1(x) = x + 0.35 \sin(4\pi x), \quad \gamma^2(x) = 2 + \sin(2\pi(x - 0.25)), \quad x \in [0, 1].$$

344 Table 5 summarizes the results obtained in this case.

Table 3
The condition numbers for (4.2) and $badA$

	c_0	c_1
$m = 6$	2.4995	1.7830×10^3
$m = 7$	2.5822	3.4932×10^3
$m = 8$	2.6958	1.4214×10^4
$m = 9$	2.8223	5.6588×10^4
$m = 10$	2.9205	2.3298×10^5

Table 4
The condition numbers for (4.2) and $badA$

	c_0	c_1
$m = 6$	23.0605	7.3683×10^2
$m = 7$	24.5880	2.9023×10^3
$m = 8$	25.6142	8.6849×10^3
$m = 9$	9.2017	4.3001×10^4
$m = 10$	13.1765	1.8960×10^5

Table 5

The condition numbers for (4.2) and *badA*

	c_0	c_1
$m = 6$	48.1249	7.8616×10^1
$m = 7$	46.2576	7.9994×10^2
$m = 8$	46.2058	2.7657×10^3
$m = 9$	22.3886	1.1394×10^5
$m = 10$	12.9137	6.6306×10^5

345 It should be observed that the condition number of *badA* grows as the discretization becomes finer since
 346 the problem is ill-posed. Looking at the condition number c_0 we see that our preconditioning procedure
 347 really achieves its goal, since the condition number doesn't virtually grow anymore and is therefore all
 348 confined to the simple operator $\text{op}_m(a_0)$. The second and third example suggest that a large variation in the
 349 boundary curve is actually worse than a lack of smoothness, at least in terms of the numerical properties.
 350 This is not completely unexpected since it becomes more and more difficult to capture the nonlocal con-
 351 tribution from different spots along the curve due to the fact that, in the large variation case, their con-
 352 tributions are many orders of magnitude apart from one another.

353 **Remark 7.** We point out that, even though the proposed preconditioning method is original, other pre-
 354 conditioning techniques have previously been used for single layer potentials in the context of boundary
 355 elements methods, see [6,10].

356 4.2. The method is very accurate

357 Next we take on the above examples again and actually compute the DtN operator and compare to the
 358 exact solution to illustrate the accuracy of the method we introduced. It should be clear that the method
 359 ought to be very accurate by construction. To show that we compute both the relative L_2 and the L_∞ -norms.
 360 After that we compute DtN for generic curves and boundary data to show its stability with respect to
 361 variations of the domain geometry.

362 Let us fix

$$h(x, y) = e^{-2\pi y} \cos(2\pi x) + 100e^{-6\pi y} \cos(6\pi x) + e^{-12\pi y} \cos(12\pi x)$$

364 as the harmonic function we use to produce the exact Neumann datum $\text{DtN}(g)$ to the boundary value

$$g(x) = h(x, s(x)), \quad x \in [0, 1] \quad (4.3)$$

366 along the boundary curve s . Let also

$$u = \text{DtN}(g) \quad \text{and} \quad u_m = \text{DtN}_m(g_m)$$

368 denote the exact and the approximate solution, respectively. We compute the relative $L_{2,p}(0, 1)$ and
 369 $L_{\infty,p}(0, 1)$ -errors

$$e_m^2 = \frac{\|u - u_m\|_{L_2}}{\|u\|_{L_2}} = \sqrt{\frac{\sum_{j=0, \dots, n-1} |u(j * h) - u_m(j)|^2}{\sum_{j=0, \dots, n-1} |u(j * h)|^2}}$$

371 and

$$e_m^\infty = \frac{\|u - u_m\|_{L_\infty}}{\|u\|_{L_\infty}} = \frac{\max_{j \in \{0, \dots, n-1\}} |u(j * h) - u_m(j)|}{\max_{j \in \{0, \dots, n-1\}} |u(j * h)|}$$

Table 6

The relative error for s as in 1 and for (4.3)

	e_m^2	e_m^∞
$m = 6$	6.1303×10^{-9}	1.6655×10^{-8}
$m = 7$	4.2456×10^{-14}	1.1732×10^{-13}
$m = 8$	1.4749×10^{-13}	3.3107×10^{-13}
$m = 9$	4.5708×10^{-13}	9.6493×10^{-13}
$m = 10$	2.1229×10^{-12}	5.4297×10^{-12}

374 **Example 5.** Assume that s is given as in Example 1 and that g is determined by (4.3). We obtain the results given in Table 6

375 **Example 6.** Consider now s as given in Example 2 and g given by (4.3). Then we obtain the errors contained
376 in Table 7.

377 **Example 7.** Consider now s as given in Example 3 and g given by (4.3). The relative errors are given in
378 Tables 8 and 9 for $\alpha = 4$ and for $\alpha = 15$, respectively.

379 **Example 8.** Consider now Γ as specified in Example 4 and g given by (4.3). We obtain the errors shown in
380 Table 10.

Table 7

The relative error for s as in 2 and for (4.3)

	e_m^2	e_m^∞
$m = 6$	8.9405×10^{-2}	1.0894×10^{-1}
$m = 7$	7.1529×10^{-3}	8.5876×10^{-3}
$m = 8$	3.8747×10^{-5}	5.1342×10^{-5}
$m = 9$	1.1816×10^{-9}	1.7387×10^{-9}
$m = 10$	1.7506×10^{-13}	9.9333×10^{-13}

Table 8

The relative error for s as in 3 and for (4.3)

	e_m^2	e_m^∞
$m = 6$	7.1434×10^{-6}	7.5789×10^{-6}
$m = 7$	1.3932×10^{-7}	1.9187×10^{-7}
$m = 8$	2.2859×10^{-9}	4.0785×10^{-9}
$m = 9$	3.4170×10^{-11}	9.1362×10^{-11}
$m = 10$	2.4456×10^{-12}	4.1165×10^{-12}

Table 9

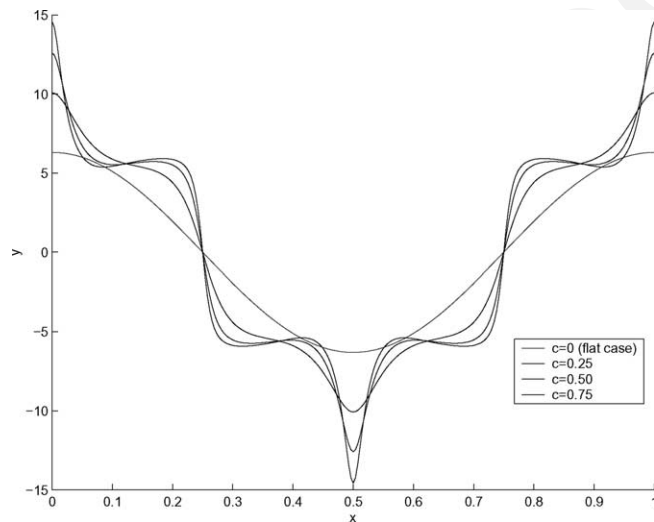
The relative error for s as in 2 and for (4.3)

	e_m^2	e_m^∞
$m = 6$	4.7471×10^{-5}	5.3208×10^{-5}
$m = 7$	7.5167×10^{-10}	3.5195×10^{-10}
$m = 8$	2.5880×10^{-13}	3.6613×10^{-13}
$m = 9$	7.8558×10^{-13}	1.4393×10^{-12}
$m = 10$	3.2135×10^{-12}	6.1163×10^{-12}

Table 10

The relative error for s as in 2 and for (4.3)

	e_m^2	e_m^∞
$m = 6$	2.3240×10^{-3}	2.3202×10^{-3}
$m = 7$	1.0230×10^{-5}	1.4338×10^{-4}
$m = 8$	1.2225×10^{-6}	2.1721×10^{-6}
$m = 9$	1.4307×10^{-9}	2.8500×10^{-9}
$m = 10$	1.6602×10^{-13}	2.3675×10^{-13}

Fig. 4. The function $\text{DtN}(cs, g)$ for different values of c .

381 The above examples show clearly that our method is very accurate, is stable in the sense explained and
 382 performs well even for curves which are nonsmooth and/or of large variation. The method appears to be
 383 spectrally accurate. Finally we would like to present an example where we freely choose both the curve s
 384 determining the boundary and the boundary datum g .

385 **Example 9.** Let us use s as given in Examples 2 and 6 and the boundary function

$$g(x) = \cos(2\pi x), \quad x \in (0, 1).$$

387 In Fig. 4 we show $\text{DtN}(cs, g)$ for different values of $c \geq 0$ starting with the flat case for fixed discretization
 388 parameter $m = 8$.

389 5. Conclusion

390 We proposed a boundary integral method for the computation of the Dirichlet-to-Neumann operator in
 391 the 2D periodic case using ΨDO and explicit representations of the integral operators involved via periodic
 392 kernels. In the process we showed that there is a lot of freedom in the choice of the kernel to be used for the
 393 integral equations involved and how to produce appropriate periodic kernels solely by means of their flat
 394 symbols and the jump relation for their continuous counterparts. On this basis we suggested a discretization

395 method which works very well for curves which can be both nonsmooth and/or of large variation proving
396 to be spectrally accurate. We proposed a preconditioning procedure for an integral equation of first kind
397 which we therefore can accurately solve without resorting to special quadrature or regularization tech-
398 niques. Finally we corroborated our analysis with a series of numerical examples which show the great
399 benefits obtained.

400 The method developed here for the DtN operator appears very general and applicable to a variety of ill-
401 posed integral equations. It also appears possible to use a similar procedure in 3D. We shall be addressing
402 these issues in a forthcoming paper.

403 Acknowledgements

404 The author wishes to thank Hector Cenicerros for interesting discussions and helpful suggestions.

405 Appendix A

406 **Proof of Lemma 4.** Let R_α denote the rotation

$$R_\alpha = \begin{bmatrix} \cos(\alpha) & -\sin(\alpha) \\ \sin(\alpha) & \cos(\alpha) \end{bmatrix}$$

408 of angle $\alpha \in (-\pi/2, \pi/2)$ about the origin. We prove the claim for

$$(x_\varepsilon, y_\varepsilon) = (x_0, y_0) + \varepsilon R_\alpha(-s_x(x_0), 1) \in \Omega_\Gamma$$

410 letting $\varepsilon \rightarrow 0+$. Any general nontangential approximating sequence is in fact contained in a wide enough
411 cone. Since the kernel is smooth away from the boundary curve we can consider

$$I_{0 \leq \tilde{x} \leq 1}(\varepsilon) := \int_0^1 K(x, \tilde{x}) f(\tilde{x}) \sqrt{\frac{1 + s_x^2(\tilde{x})}{1 + s_x^2(x_0)}} d\tilde{x}$$

413 for

$$K(x, \tilde{x}, \varepsilon) = (s_x(x_0), -1) \cdot \nabla G(x_\varepsilon, y_\varepsilon).$$

415 Taking the limit as ε goes to 0 will produce the boundary value. The limit only exists on a regularity
416 assumption for f . Here we think of f as being continuous but a natural assumption in the $L_{2,p}$ context
417 would be $f \in H_p^{1/2}(\Gamma)$. We then split the integral into two pieces as follows

$$I_{0 \leq \tilde{x} \leq 1}(\varepsilon) = I_{|x_0 - \tilde{x}| \leq \sqrt{\varepsilon}} + I_{|x_0 - \tilde{x}| > \sqrt{\varepsilon}}, \quad (\text{A.1})$$

419 where the distance $|x_0 - \tilde{x}|$ is to be measured modulo the period, that is,

$$|x_0 - \tilde{x}| := x_0 - \tilde{x} \bmod 1.$$

421 Using (2.20) it is easily checked that

$$\nabla G(x, y) = \frac{1}{\pi} \left(\frac{x}{x^2 + y^2}, \frac{y}{x^2 + y^2} \right) + (r_1(x, y), r_2(x, y)) \quad (\text{A.2})$$

423 for bounded functions r_i , $i = 1, 2$. It therefore follows that

$$I_{|x_0-\tilde{x}|>\sqrt{\varepsilon}}$$

$$\downarrow \quad (\varepsilon \rightarrow 0)$$

$$v.p. \int_0^1 K(x_0, \tilde{x}) f(\tilde{x}) \sqrt{\frac{1+s_x^2(\tilde{x})}{1+s_x^2(x_0)}} d\tilde{x}$$

427 for

$$K(x_0, \tilde{x}) = -\partial_y G(x_0 - \tilde{x}, s(x_0) - s(\tilde{x})) + s_x(x_0) \partial_x G(x_0 - \tilde{x}, s(x_0) - s(\tilde{x})).$$

429 As to the first term in (A.1) we proceed as follows. Since f is smooth and $s_x \in C_p([0, 1])$ it follows from
430 (2.20) or (A.2) that

$$\int_{|x_0-\tilde{x}| \leq \sqrt{\varepsilon}} K(x_0, \tilde{x}, \varepsilon) \left[f(\tilde{x}) \sqrt{\frac{1+s_x^2(\tilde{x})}{1+s_x^2(x_0)}} - f(x_0) \right] d\tilde{x}$$

432 converges to zero. Hereby we clearly set

$$K(x_0, \tilde{x}, \varepsilon) = (s_x(x_0), -1) \cdot \nabla G(x_\varepsilon, y_\varepsilon).$$

434 We therefore only need to analyse

$$\int_{|x_0-\tilde{x}| \leq \sqrt{\varepsilon}} K(x_0, \tilde{x}, \varepsilon) f(x_0) d\tilde{x}.$$

436 Using (A.2) we see that

$$K(x_0, \tilde{x}, \varepsilon) \approx -\frac{1}{\pi} \frac{-s(x_0)a_1(x_0, \tilde{x}, \varepsilon) + a_2(x_0, \tilde{x}, \varepsilon)}{a_1^2(x_0, \tilde{x}, \varepsilon) + a_2^2(x_0, \tilde{x}, \varepsilon)},$$

438 where

$$a_1(x_0, \tilde{x}, \varepsilon) = x_0 - \tilde{x} - \varepsilon[s_x(x_0) \cos(\alpha) + \sin(\alpha)]$$

440 and

$$a_2(x_0, \tilde{x}, \varepsilon) = s(x_0) - s(\tilde{x}) + \varepsilon[-s_x(x_0) \sin(\alpha) + \cos(\alpha)].$$

442 Now, taking into account the differentiability of s we obtain after some manipulation

$$K(x_0, \tilde{x}, \varepsilon) \approx -\frac{1}{\pi} \frac{\varepsilon \cos(\alpha)}{(x_0 - \tilde{x} - \varepsilon \sin(\alpha))^2 + \varepsilon^2 \cos^2(\alpha)}. \tag{A.3}$$

444 When we write $f \approx g$ we mean that $f - g$ is a at least integrable function. It is therefore an easy
445 computation to see that

$$\lim_{\varepsilon \rightarrow 0^+} \int_{|x_0-\tilde{x}| \leq \sqrt{\varepsilon}} K(x_0, \tilde{x}, \varepsilon) f(x_0) d\tilde{x} = -f(x_0)$$

447 follows from (A.3) provided $\alpha \in (-\pi/2, \pi/2)$. In conclusion, putting all the pieces back together we obtain
448 the claimed formula. \square

449 **Appendix B. Kernel derivation from the flat symbol**

450 In general one cannot expect to obtain explicit representations for the kernel like (2.2). It is therefore
451 important and interesting to obtain a representation of the nonflat kernel in terms of the symbol of its flat
452 counterpart.

453 The DtN operator in the flat case can be viewed as a Ψ DO with constant coefficients and symbol

$$d_0 = (2\pi|k|)_{k \in \mathbb{Z}}$$

455 or, equivalently, the “boundary operator” of the operator family with symbols

$$d_0(\cdot, y) = \left(\begin{bmatrix} 2\pi i k \\ -2\pi |k| \end{bmatrix} \cdot \begin{bmatrix} 0 \\ -1 \end{bmatrix} e^{-2\pi |k| y} \right)_{k \in \mathbb{Z}}, \quad y > 0,$$

457 which corresponds to the symbol of the periodic Poisson kernel. It seems therefore natural to view the DtN
458 operator for a generic curve as the Ψ DO with nonconstant coefficients with symbol

$$d(\cdot, x, \tilde{x}) = \left(\begin{bmatrix} 2\pi i k \\ -2\pi |k| \end{bmatrix} \cdot \begin{bmatrix} v_1(x) \\ v_2(x) \end{bmatrix} e^{-2\pi |k| (s(x) - s(\tilde{x}))} \right)_{k \in \mathbb{Z}}, \quad x, \tilde{x} \in [0, 1)$$

460 using the standard notation for Ψ DOs (see [4] for instance) and denoting the unit outer normal to Γ at
461 $x \in \Gamma$ with $v(x)$. The latter is simply the “normal derivative symbol” of

$$a(\cdot, x, \tilde{x}) = \left(e^{-2\pi |k| (s(x) - s(\tilde{x}))} \right)_{k \in \mathbb{Z}}, \quad x, \tilde{x} \in [0, 1),$$

463 restricted to the boundary. The kernel

$$K(x, \tilde{x}) = H(x - \tilde{x}, s(x) - s(\tilde{x})), \quad x, \tilde{x} \in [0, 1),$$

465 seems to be directly associated to this symbol via

$$K(x, \tilde{x}) = \sum_{k \in \mathbb{Z}} e^{-2\pi |k| (s(x) - s(\tilde{x}))} e^{2\pi i k (x - \tilde{x})}.$$

467 Unfortunately this point of view seems hopelessly formal in view of the terrible lack of convergence of
468 the above series. The difference $s(x) - s(\tilde{x})$ can and, in fact, always will assume both positive and negative
469 values unless the curve is flat. We now show how this point of view can be safely maintained with the
470 necessary modifications.

471 **Theorem 8.** *The Fourier symbol of the operator with kernel K for a generic curve (of graph type) is given by*

$$a(k, x, \tilde{x}) = e^{-2\pi |k| (s(x) - s(\tilde{x}))}$$

473 *if*

$$k \in \mathbb{Z}, \quad x, \tilde{x} \in [0, 1) \text{ s.t. } s(x) - s(\tilde{x}) \geq 0$$

475 *and by*

$$a(k, x, \tilde{x}) = -2\delta(k) - e^{2\pi |k| (s(x) - s(\tilde{x}))}$$

477 *if*

$$k \in \mathbb{Z}, \quad x, \tilde{x} \in [0, 1) \text{ s.t. } s(x) - s(\tilde{x}) < 0.$$

Proof. Whenever the “natural” series converges it obviously sums up to

$$H(x - \tilde{x}, s(x) - s(\tilde{x})).$$

481 Now, H is also well-defined in the lower half plane and its values for negative second argument are
482 precisely those we need to complete the definition of our symbol in the appropriate way. Fortunately, the
483 values of H in the lower complex half-plane are uniquely determined by those in the upper half-plane. In
484 fact H enjoys the symmetry property

$$H(x, -y) + H(x, y) = -2, \quad x \in \mathbb{R}, \quad y > 0. \quad (\text{B.1})$$

486 Since H is known explicitly, this can be checked by a simple calculation. It is therefore clear how the
487 symbol needs to be defined for

$$s(x) - s(\tilde{x}) < 0$$

489 in order to produce the right kernel. \square

490 **Remark 9.** In most cases (like for the DtN operator in 3D) one cannot produce an explicit formula for the
491 kernel. It is therefore crucial to understand how the definition of the “right symbol” has to be made based
492 on available knowledge. The latter consists of the “convergent part” of the series and of the singularity in
493 the origin, which coincides with the one of the continuous flat geometry kernel. The free space version of H
494 is given by

$$H_f(x, y) = \frac{1}{\pi} \frac{y}{x^2 + y^2}, \quad x \in \mathbb{R}, \quad y \neq 0,$$

496 and satisfies the well-known jump-relation

$$\lim_{y \rightarrow 0_{\pm}} H_f(x, y) = \pm \delta \text{ in } \mathcal{S}'(\mathbb{R}).$$

498 It follows directly from the Fourier series representation of H that

$$\lim_{y \rightarrow 0^+} H(x, y) = \delta - 1.$$

500 Since the jump-relation is determined by the singularity, which, in turn, is determined by the “continuous
501 kernel” we obtain the following jump relation for the periodic kernel

$$\lim_{y \rightarrow 0_{\pm}} H(x, y) = \pm \delta - 1,$$

503 which leads to the symmetry property (B.1) in the limit as $y \rightarrow 0$. The property extends to the whole
504 complex plane since $H(\cdot, \cdot) + H(\cdot, -\cdot) \equiv -2$ is the unique continuous bounded harmonic function with
505 value -2 on the real line by Liouville’s theorem.

506 The same analysis can be performed for the kernel G , given by (2.2). Its symbol is then seen to be given
507 by

$$g(k, x, \tilde{x}) = \frac{e^{-2\pi|k|(s(x)-s(\tilde{x}))}}{2\pi k} \quad (\text{B.2})$$

509 if

$$k \in \mathbb{Z}, \quad x, \tilde{x} \in [0, 1) \text{ s.t. } s(x) - s(\tilde{x}) \geq 0$$

511 and by

$$g(k, x, \tilde{x}) = \frac{e^{2\pi i k |s(x) - s(\tilde{x})|}}{2\pi k} + e^{2\pi i k \tilde{x}} \hat{c}(k, \tilde{x}) \quad (\text{B.3})$$

513 if

$$k \in \mathbb{Z}, \quad x, \tilde{x} \in [0, 1) \text{ s.t. } s(x) - s(\tilde{x}) < 0,$$

515 where the correction term \hat{c} is given by

$$\hat{c}(\cdot, \tilde{x}) = \mathcal{F}_{x \rightarrow k} c(\cdot, \tilde{x})$$

517 for

$$c(x, \tilde{x}) = -2 \left(s(x) - s(\tilde{x}) \right) \chi_{[s(x) - s(\tilde{x}) < 0]}$$

519 χ_S being the characteristic function of the set S .

520 References

- 521 [1] J.T. Beale, T.Y. Hou, J. Lowengrub, Stability of boundary integral methods for water waves, in: Nonlinear Evolutionary Partial
522 Differential Equations (Beijing, 1993), AMS/IP Stud. Adv. Math., vol. 3, American Mathematical Society, Providence, RI, 1997,
523 pp. 1–7–127.
- 524 [2] J.T. Beale, T.Y. Hou, J.S. Lowengrub, Convergence of a boundary integral method for water waves, SIAM J. Numer. Anal. 33 (5)
525 (1996) 1797–1843.
- 526 [3] R.R. Coifman, Y. Meyer, Nonlinear harmonic analysis and analytic dependence, in: F. Trèves (Ed.), Pseudodifferential Operators
527 and Applications, Proceedings of Symposia in Pure Mathematics, vol. 43, American Mathematical Society, Providence, RI, 1985,
528 pp. 71–79.
- 529 [4] H.O. Cordes, The Technique of Pseudodifferential Operators, London Mathematical Society Lecture Note Series, vol. 202,
530 Cambridge University Press, Cambridge, 1995.
- 531 [5] W. Craig, S. Sulem, Numerical simulation of gravity waves, J. Comput. Phys. 108 (1) (1993) 73–83.
- 532 [6] S.A. Funken, E.P. Stephan, The bpx preconditioner for the single layer potential operator, Appl. Anal. 67 (1997) 327–340.
- 533 [7] D. Givoli, Numerical Methods for Problems in Infinite Domains, Elsevier, Amsterdam, 1992.
- 534 [8] T.Y. Hou, J.S. Lowengrub, M.J. Shelley, Boundary integral methods for multicomponent fluids and multiphase materials, J.
535 Comput. Phys. 169 (3) (2001) 302–362.
- 536 [9] F. John, Partial Differential Equations, Springer, New York, 1982.
- 537 [10] M. Kamon, M.J. Tsuk, J. White, Fasthenri: a multipole-accelerated 3-d inductance extraction program, IEEE Trans. Microw.
538 Theory and Techniques (1994).
- 539 [11] A. Kirsch, An Introduction to the Mathematical Theory of Inverse Problems, Applied Mathematical Sciences, vol. 120, Springer,
540 New York, 1996.
- 541 [12] A. McKenney, L. Greengard, A. Mayo, A fast poisson solver for complex geometries, J. Comput. Phys. 118 (2) (1995) 348–355.
- 542 [13] D.M. Milder, An improved formalism for electromagnetic scattering from a perfectly conducting rough surface, Radio Sci. 31 (6)
543 (1996) 1369.
- 544 [14] D.P. Nicholls, F. Reitich, Stability of high-order perturbative methods for the computation of Dirichlet–Neumann operators, J.
545 Comput. Phys. 170 (2001) 276–298.
- 546 [15] A. Sidi, M. Israeli, Quadrature methods for periodic singular and weakly singular Fredholm integral equations, J. Sci. Comput. 3
547 (1988) 201.
- 548 [16] M.E. Taylor, Tools for PDE, Mathematical Surveys and Monographs, vol. 81, American Mathematical Society, Providence, RI,
549 2000.